Thin Solid Films 688 (2019) 137349

Contents lists available at ScienceDirect

Thin Solid Films

journal homepage: www.elsevier.com/locate/tsf

Stabilizing effects of oxidation on propagating formation reactions occurring in nanometer-scale metal multilayers

D.P. Adams*, M.J. Abere, C. Sobczak, M.A. Rodriguez

Sandia National Laboratories, Albuquerque, NM 87185, USA

ARTICLE INFO

Keywords:
Thin film
Sputter deposition
Reactive multilayer
Exothermic
Self-propagating reaction

ABSTRACT

Reactive rare-earth/transition metal multilayers exhibit a variety of complex reaction behaviors depending on surrounding gaseous environment and material design. Small period (< 100 nm bilayer), 5 μm-thick Sc/Ag multilayers undergo self-sustained formation reactions when ignited in air or in vacuum. High-speed videography reveals unstable reaction waves in these samples, characterized by the repeated, transverse passage of narrow, spin bands. Intermediate Sc/Ag designs – with multilayer period between 100 and 200 nm – only react in air. These multilayers exhibit propagating reactions with alternating unstable and stable characteristics. Narrow, spin bands advance the reaction front stepwise. Soon after the passage of a transverse band, a trailing oxidation wave encroaches on the intermetallic reaction front temporarily pushing the stalled wave forward in a uniform manner. Viewed in full, these events repeat giving rise to a new oscillatory behavior. Sc/Ag multilayers having a large period (> 200 nm bilayer) also react exclusively in air but exhibit a different propagating mode. The oxidation of Sc combined with the exothermic reaction of metal species results in continually-stable waves characterized by a smooth wavefront morphology and uniform velocity. The flame temperatures associated with propagating waves are estimated using measured heats of reaction and enthalpy-temperature relationships in order to provide insight into the possible phase transformations that occur during these different exothermic reactions.

1. Introduction

Propagating chemical reactions that occur within energetic thin films provide opportunity to investigate phase transformations subject to high heating rates up to 10^7 °C/s [1]. Amorphous films that undergo 'explosive' crystallization [2–4] and multilayers that exhibit rapid formation reactions [1,5–7] have been the subjects of such investigation in past years, and their study has revealed new details regarding the underlying atomic-scale processes. Both types of energetic films are stimulated at single points to initiate internal exothermic reactions. Once ignited, a self-sustained, high-temperature, propagating reaction ensues driven by rapid internal heat release. Propagating reaction waves moving laterally through these films are often characterized by time-resolved videography, pyrometry, or diffraction-based techniques. The obtained information is contrasted with predictions from numerical and/or analytical model simulations to elucidate the thermodynamic and kinetic factors affecting transformation.

Both stable and unstable reaction waves have been observed in energetic thin films. A stable reaction wave is often identified by a uniformly advancing front and single radial velocity. An unstable wave does not advance uniformly, and its radial velocity may vary over time. Unstable reactions appear as oscillatory, spinning, or chaotic waves [8–12]. A few models have been developed to predict reaction wave stability in these materials [13–16]. Notably, it has been >35 years since a thermal instability model [13] for explosive crystallization was confirmed by Wickersham, Bajor, and Greene [17].

Despite improved knowledge of the atomic-scale processes that underlie propagating reactions, the unstable modes occurring in reactive multilayers remain poorly understood. In particular, little is known about 2-D (spin) instabilities that develop in low heat release multilayers. As depicted in Fig. 1, this instability is characterized by a reaction wave that spirals in the plane of a film about an axis of rotation normal to the multilayer located at the ignition site [9]. Generally, the reaction wave stalls in the radial, or net propagation, direction. However, the reaction continues by the repeated passage of narrow reaction bands along the boundary of previously reacted volumes of the multilayer. A previous study predicts that this type of 2-D instability develops when the forward heat transfer rate lies below a critical, material-specific value [11], but additional research is needed to confirm said effect.

* Corresponding author.
E-mail address: dpadams@sandia.gov (D.P. Adams).

https://doi.org/10.1016/j.tsf.2019.05.068
Received 24 April 2019; Received in revised form 31 May 2019; Accepted 31 May 2019
Available online 12 June 2019
0040-6090/ © 2019 Published by Elsevier B.V.

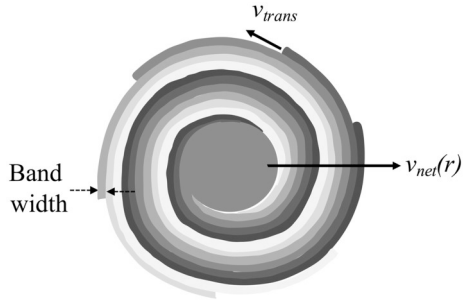


Fig. 1. Depiction of the reaction wave instability observed during some propagating reactions in Sc/Ag multilayer foils. Ignition occurs at the center of the material and narrow, reaction bands propagate with speed v_{trans} around the boundary of previously-reacted material. The speed, v_{net}, represents the average radial velocity in the net forward direction. The different shades of gray are used to distinguish the individual spin bands. In this plan view depiction, the individual reactant layers lie in the plane of the page.

The current investigation explores the effects of surrounding gaseous environment on wave stability in reactive metal multilayers. At the onset of research, we postulated that certain metal reactants found in multilayers may oxidize soon after intermetallic formation and this additional reaction (with air) could have a pronounced effect on the local heating rate in proximity of a propagating intermetallic wave. Building on the idea of Reeves et al. [11] that a critical heat transfer rate is needed to achieve stability, it was expected that certain intermetallic reaction waves could be stabilized if oxidation occurred promptly. Oxidation of metal species is often characterized by a large enthalpy of formation compared with the heat associated with intermetallic compound formation. Thus, it was anticipated that secondary combustion occurring in neighboring volumes would provide substantial added heat [18–20]. Increased stability was also considered feasible based on a prior study that correlated enhanced wave stability with increased ambient temperature [11].

Vapor-deposited Sc/Ag multilayers were chosen for this study of wave stability and environmental effects. Unstable propagating reactions are known to develop in Sc/Ag multilayers, and these materials exhibit a spin-like character [21]. Additionally, the system was selected because one of the reactants (Sc) has a strong affinity for oxygen. The reaction enthalpy of $4Sc + 3O_2 -> 2Sc_2O_3$ (-20.9 kJ/g) [22] is considerably larger than that of Sc + Ag- > ScAg (-0.32 kJ/g) [23,24], so there is a thermodynamic basis to expect scandium oxidation when ignited in air. A question remained: would oxidation occur promptly in a manner that influences wave stability in this system? Our approach to answering this question involves testing various Sc/Ag multilayers having different design. Multilayers were made with different period in order to gain access to a range of internal heat release rates. It was expected that a wide range of internal heat release rates would provide opportunity for prompt oxidation in some tests. In order to provide a better understanding of propagating wave stability, this manuscript also assesses the flame temperatures and possible phase evolution associated with propagating reactions in Sc/Ag. Flame temperatures are estimated from enthalpy-temperature diagrams that are constructed using measured reactive properties and archived information.

2. Experimental methods

Reactive Sc/Ag multilayers were deposited by direct current, magnetron sputtering using a Unifilm Corp. PVD-300 multi-source system. This cryopumped apparatus maintains a base pressure of 1.33×10^{-5} Pa (1×10^{-7} Torr) to facilitate the growth of pure metals. High-purity Sc (99.99%) and Ag (99.99%) targets were pre-sputtered prior to the start of multilayer deposition in order to remove oxide layers and adventitious carbon. These targets were configured in a sputter-down geometry with a working distance of 1 cm. Sputtering employed ultra-high purity (99.999%) Ar gas maintained at a pressure of 1.33 Pa (10 mTorr) as measured by a capacitance manometer. Multilayer films were deposited onto oxidized Si(100) wafers which were rotated and translated under sputter targets to establish uniform layer thicknesses. Deposition rates were calibrated prior to multilayer growth using a DEKTAK™ surface profilometer and scanning electron microscopy (SEM) employing focused ion sectioning.

Table 1
Total released heat and measured activation energies for reaction of various Sc/Ag multilayers Results are determined from DSC.

Bilayer thickness	Bilayer number	Total ΔH_{rxn} [kJ/mol.at.]	E_a [kJ/mol.at.]
20.8 nm	240	−18.1 ± 0.7	n/m
23.8 nm	210	−18.3 ± 0.9	n/m
27.8 nm	180	−18.8 ± 1.2	n/m
33.3 nm	150	−19.2 ± 0.9	138.6 ± 5.0
41.7 nm	120	−21.8 ± 0.6	138.7 ± 6.0
62.5 nm	80	−22.7 ± 1.1	128.8 ± 6.0
83.3 nm	60	−22.7 ± 1.3	117.9 ± 5.2
125 nm	40	−23.3 ± 1.1	132.4 ± 7.0
166.7 nm	30	−23.4 ± 1.2	131.9 ± 4.5
250 nm	20	−23.5 ± 1.2	111.3 ± 6.2
357 nm	14	−23.9 ± 0.6	126.4 ± 5.6
417 nm	12	−23.9 ± 0.7	118.1 ± 7.2
500 nm	10	−23.8 ± 1.9	134.0 ± 6.5

Multilayer stoichiometry was set to an equimolar ratio (1Sc:1Ag) by commanding reactant layer thicknesses accordingly. All layer designs account for the densities of Sc (4.02×10^{22} at./cm^3) and Ag (5.86×10^{22} at./cm^3) when targeting equal amounts of metal reactants. Each multilayer was made with a single period – also referred to as a bilayer thickness (t_B). To be clear, bilayer thickness is the combined thickness of one Sc and one Ag layer. This thickness is varied in subsequent depositions to ultimately gain access to different internal heating release rates in propagating formation reactions. Total multilayer thickness was held constant at 5.0 μm. Thus, multilayers consisted of many bilayers as listed in Table 1. Silver was deposited as a first layer in order to aid the removal of multilayers from substrates. Multilayers were peeled from substrates prior to all reaction tests.

Differential scanning calorimetry (DSC) was used to obtain thermograms which were analyzed to determine the onset reaction temperature (T_{onset}) and the heat of reaction (ΔH_{rxn}) for multilayers. Approximately 4 mg of multilayer was placed in a Cu pan and sealed with a Cu lid for each test in a Perkin Elmer (PE) model 8500 calorimeter. Experiments used to determine T_{onset} and ΔH_{rxn} involved the following procedure. A sample was first heated to 600 °C at a rate of 10, 20 or 40 °C/min. and then cooled to 50 °C. Following a brief pause, a second identical heat-and-cool cycle was completed. A maximum temperature of 600 °C was chosen for calorimetry, because Sc/Ag multilayers were fully reacted after heating once to this value. Complementary X-ray diffraction (XRD) showed a B2 ScAg product phase in the various samples with no residual elemental Sc and Ag after heating. Consistently, no exotherms (or endotherms) were observed on the second identical heat-and-cool calorimeter cycles. Thus, the second heat cycle established a baseline for evaluating T_{onset} and ΔH_{rxn} using the PE Pyris™ software. Thermograms generated at different heating rates were also evaluated to determine the activation energies associated with reactions in these materials. A Kissinger approach was implemented for this latter analysis [25].

The reaction pathway associated with these low heating rates was evaluated by quenching separate multilayer samples heated once to prescribed temperatures ≤600 °C. By shutting off electrical power to the sample furnace after reaching a temperature of interest, the calorimeter's cooling block reduces sample temperature at high rates, up to about 1000 °C/min., to prevent additional phase formation. XRD was used to assess the structural changes associated with exotherms and to

generally evaluate phase in multilayers. Conventional θ-2θ XRD scans of films were obtained using a Siemens D500 diffractometer that utilizes a CuKα source, fixed slits, diffracted-beam monochromator, and scintillation detector. Micro-diffraction analysis was performed using a Bruker D8 diffractometer with a Vantec 2000 area detector and an Eulerian texture cradle. This system employed a sealed-tube (CuKα) X-ray source with an incident-beam mirror optic for removal of Kβ radiation. The samples were aligned using a video camera and laser system on the D8 instrument. A 500-μm pinhole was used as an incident-beam optic to generate a small, collimated beam for spatially-resolved, micro-XRD measurements. To be clear, calorimetry and complementary XRD of quenched samples do not necessarily reveal the phase formation pathway associated with self-propagating reaction waves. Previous work on Ni/Al multilayers has shown that the phase sequence occurring in a propagating reaction wave can be quite different than that formed at lower heating rates (involved with calorimetry) [7]. The phases formed at low heating rates are included, nevertheless, so to provide a basis for future studies.

Select multilayers were evaluated using scanning transmission electron microscopy (STEM) and SEM. Cross-section samples were prepared for electron microscopy using an FEI Co. DB-235 focused ion beam (FIB) system. STEM involved an FEI Co. Titan G2 80-200 electron microscope operated at 200 kV. This instrument incorporates a spherical aberration corrector on the probe-forming optics and four SuperX™ silicon drift detectors (SDDs). Compositional profiles were obtained from energy-dispersive spectroscopy (EDS) maps obtained in the Titan G2 electron microscope. Characterization of multilayers involved positioning samples such that two of the SDDs were aligned to look down their interfaces. SEM images were obtained using the DB-235 dual beam system.

Thermal ignition tests determined the ignition temperature (T_{ign}) of each Sc/Ag multilayer. Tests utilized an IKA C-Mag hotplate and ~1 × 1 mm^2 multilayer foil samples. Each thin specimen was dropped rapidly onto the equilibrated hotplate (in air) and observed by eye. Specimens ignited by the hotplate reacted rapidly giving off a flash of light. Unignited samples did not give off light but changed shape. Tests were repeated over a range of temperatures to identify a minimum value for ignition, reported as T_{ign}. A type K thermocouple verified the local hotplate temperature where a given specimen ignited.

High-speed videography provided a time-resolved look at self-propagating reactions. Peeled multilayers having an area of approximately 1 × 1 cm^2 were mounted across washers with tape at edges for ignition and viewing. A test chamber used to fixture samples was kept at atmospheric pressure (with air) or evacuated to 0.013 Pa (0.1 mTorr) for reactions in vacuum. Mounted samples were ignited at single points using the light emitted by a Northrup-Grumman eDrive™ diode laser. The 810 nm-wavelength light was focused to an approximate 310 μm spot diameter, steered through a viewport affixed to the test chamber, and directed onto the Sc-coated side of multilayers to start reactions. A Vision Research Phantom V12 high-speed camera captured a stream of images in plan view. Continuous fiber-optic illumination was required to visualize propagating intermetallic fronts, whereas oxidation waves emitted sufficient light to distinguish their separate wavefronts. Plots of wave position versus time obtained from videography serve to i.) identify reaction mode and ii.) determine wave speed. Additionally, wavefront position plots were evaluated to determine the time duration between individual spin bands and spin band arrival rate when unstable reactions ensue. Samples were maintained at room temperature (approximately 22 °C) prior to ignition.

3. Results

3.1. Structure and composition of deposited multilayers

A set of thin film multilayers spanning a range of t_B from ~20 to 500 nm was deposited for testing as specified in Table 1. Deposited

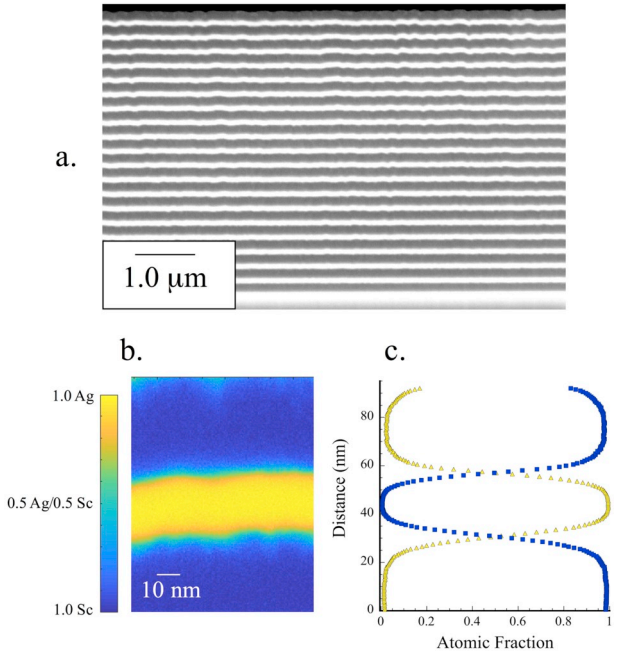


Fig. 2. (a) Cross-section SEM image of a Sc/Ag multilayer having t_B = 250 nm. This secondary electron micrograph shows alternating silver (bright) and scandium (dark) layers. Note: the appearance of the first silver layer is affected by charging in the underlying silicon dioxide substrate cap layer. The TEM/EDS composition map in (b) was obtained from a different Sc/Ag multilayer having t_B = 62.5 nm. The compositional trace in (c) was obtained from the included elemental map.

films, like the one shown in Fig. 2(a), have an alternating structure with Sc layers ~1.45× thicker than Ag layers as required for an equimolar stoichiometry. This particular film has a constant t_B = 250 nm, whereas the total thickness is approximately 5 μm. Silver layers appear bright in this cross-section SEM image, whereas scandium is relatively dark.

Structural and chemical inspection reveal high purity Sc and Ag layers. X-ray diffraction demonstrates face-centered cubic Ag and hexagonal close packed α Sc in deposited multilayers. For example, the bottom diffractogram in Fig. 3 shows multiple reflections that index to archived Ag and α Sc patterns. Furthermore, XRD demonstrates textured Ag layers with (111) planes oriented along the substrate. Scandium layers show relative diffraction intensities consistent with a random polycrystal. XRD presents no evidence for secondary intermetallic phases or oxides in deposited films. A pure deposit of Sc and Ag is consistent with prior Auger electron spectroscopy [21]. Auger spectra obtained during depth profiling revealed pure noble metal layers with only trace amounts of oxygen in Sc layers.

STEM and EDS confirm high purity metal deposits with no evidence for additional crystalline intermetallic or oxide phases. Composition maps obtained near the first few Sc/Ag layers reveal a small volume of mixed reactants at interfaces. The elemental map in Fig. 2(b) and its compositional trace in Fig. 2(c) further demonstrate a non-uniform composition through the thickness of these mixed zones. The premixed thickness is small, ~8 nm when specifying compositional boundaries of 15 and 85 at.% Ag. Complementary high-resolution TEM images obtained from these same regions were used to evaluate interfacial structure. Fourier transforms generated from these images revealed a small, planar, amorphous volume within the mixed Sc and Ag. A broad, diffuse diffraction ring characteristic of a disordered structure was obtained when sampling 4 × 4 nm^2 areas centered within premixed volumes.

Nanoscale interfacial roughness can complicate interpretation of compositional maps like that in Fig. 2(b). Recognizing this difficulty, TEM specimens were made thin and only the first few (relatively flat)

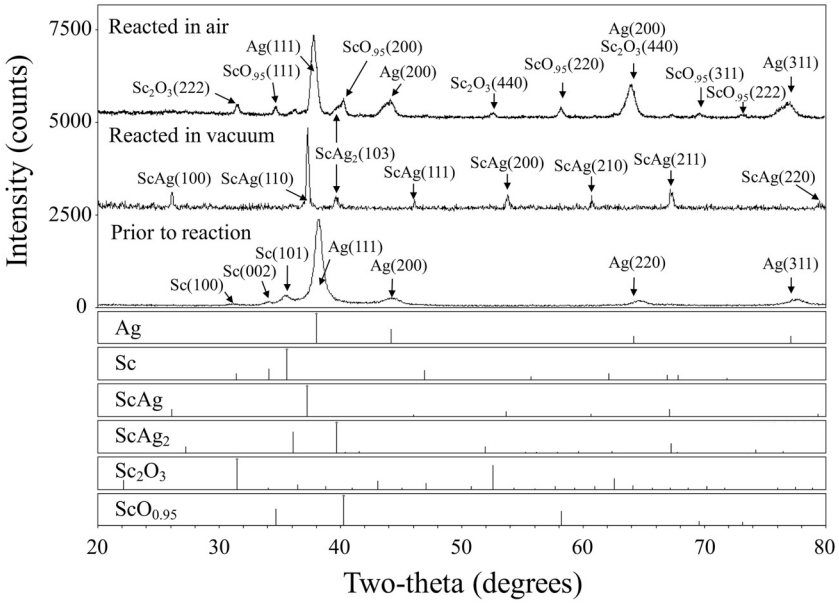


Fig. 3. X-ray diffractograms obtained from a 41.7 nm-bilayer thickness Sc/Ag multilayer prior to its reaction, after reaction in vacuum, and after rection in air. Archived information is obtained from the International Centre for Diffraction Data (ICDD) repository.

interfaces were analyzed to determine the extent of mixing. Reactant mixing at interfaces is attributed to diffusion at the deposition temperature and high energy ion/neutral species bombardment during deposition.

3.2. Calorimetry and phase evolution at low heating rates

Representative thermograms obtained from several different Sc/Ag multilayers are included in Fig. 4 with exotherms oriented downward. Multiple exotherms are evident in each test with the initial one appearing at a low temperature of ~215 °C. The additional exotherms are observed at higher temperatures. For example, the 23.8 nm bilayer Sc/Ag exhibits second and third exotherms at 250 and ~330 °C, respectively. The onset temperatures for the three exotherms shift to slightly higher values with increasing bilayer thickness similar to prior studies of vapor-deposited multilayers [10,26]. In general, no endotherms were detected.

Samples quenched after heating to prescribed temperatures have been examined to correlate the exotherms with structural changes. XRD and STEM show that phase evolves at low heating rates as follows:

$$Sc + Ag \underset{220C}{\rightarrow} Sc + Ag + aSc_xAg_y \underset{280C}{\rightarrow} ScAg_2 + Sc + Ag \underset{350C}{\rightarrow} ScAg_2 + ScAg \underset{380C}{\rightarrow} ScAg + ScAg_2(trace). \quad (1)$$

Note: the temperatures listed in Eq. (1) are associated with the 62.5 nm-bilayer Sc/Ag. Although slightly different onset temperatures are found for other multilayers, Eq. (1) serves to represent the general phase sequence observed in all tested Sc/Ag multilayers. The first low energy exotherm is correlated with the growth of an amorphous scandium-silver phase (designated as 'aSc_xAg_y'). Evidence for an amorphous interlayer composed of Sc and Ag comes primarily from STEM and EDS. STEM/EDS demonstrated a small amount of amorphous, mixed Sc and Ag in as-deposited multilayers. Therefore, Eq. (1) indicates the growth of this disordered phase at moderate temperatures that exceed the deposition temperature (estimated to be 65 °C). Both metal reactants persist up to temperatures of at least 280 °C. Crystalline $ScAg_2$ has formed at 280 °C, co-existing with residual Ag and Sc. Crystalline Ag and Sc are no longer present after the temperature has been raised to 350 °C. Instead, at this temperature this multilayer has transformed to a mixture of $ScAg_2$ and ScAg. B2 ScAg is the primary phase upon heating to 380 °C and higher temperatures.

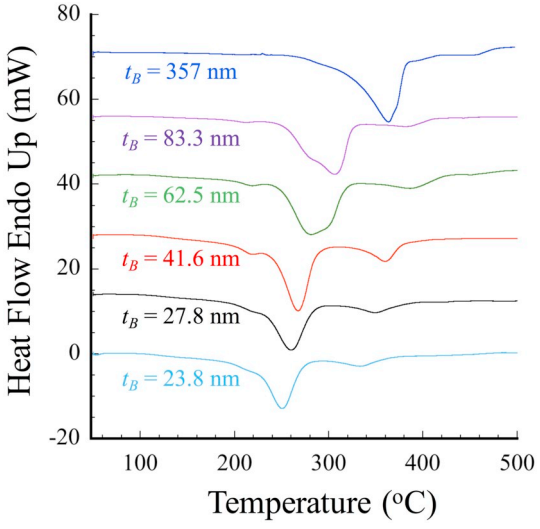


Fig. 4. DSC thermograms for Sc/Ag multilayers having different t_B. Each test was completed in flowing N_2 using a heating rate of 40 °C/min.

The effective activation energy, E_a, associated with reactions has been determined from the initial exotherms revealed by calorimetry. Implementing a Kissinger approach, E_a is determined from the measured onset temperatures using the equation,

$$ln\left(\frac{\beta}{T_{onset}^2}\right) = constant - \left(\frac{E_a}{RT_{onset}^2}\right), \quad (2)$$

wherein β is heating rate and R is the universal gas constant. Listed in Table 1, the activation energies vary from 111 to 138 kJ/mol.at. with no discernible trend. The average E_a is 126 ± 9 J/mol.at. It is noted that an E_a was not determined from several small bilayer materials, because the onset of the first exotherm, apparent in thick-bilayer designs, could not be identified with confidence. Effective activation energy should be viewed as a bulk material characteristic reflecting the interfacial chemistry, environmental conditions including ambient temperature, and initial physical configuration. It is also understood that this E_a is characteristic of low heating rates (such as those used for calorimetry)

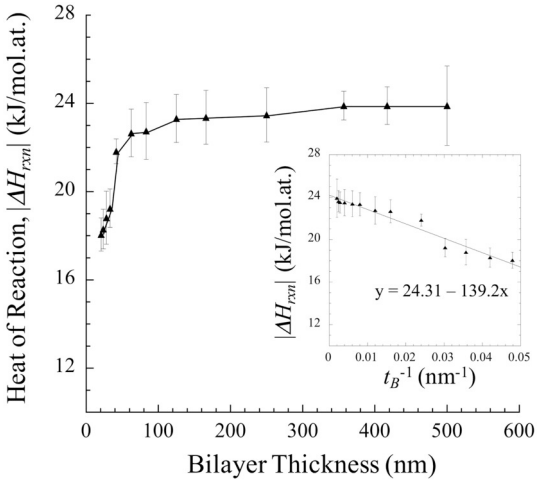


Fig. 5. Total heat released from various Sc/Ag multilayers. Inset plot graphs $|\Delta H_{rxn}|$ versus inverse bilayer thickness (t_B^{-1}).

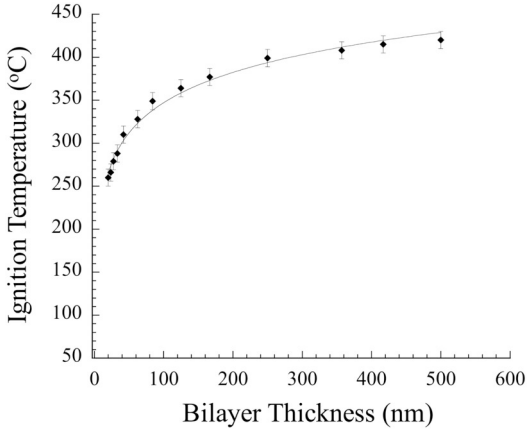


Fig. 6. Plot of T_{ig} for equimolar Sc/Ag multilayers made with different bilayer thickness. The line is a logarithmic fit.

which are substantially less than those established in propagating reactions.

Calorimetry also provides estimates for the total heat evolved from multilayers. Plotted in Fig. 5 and summarized in Table 1, the total heat of reaction in Sc/Ag multilayers is found to vary with bilayer thickness. Coarse multilayers ($t_B > 100$ nm) have the largest $|\Delta H_{rxn}|$, with average values between 23 and 24 kJ/mol.at. The $|\Delta H_{rxn}|$ is reduced as t_B is made <100 nm. For example, the 20.8 nm-bilayer Sc/Ag exhibited the lowest $|\Delta H_{rxn}| = 18$ kJ/mol.at. A reduced $|\Delta H_{rxn}|$ in small t_B Sc/Ag is attributed to premixed volumes of Sc and Ag near reactant layer interfaces. Preliminary mixing at interfaces leads to a reduced chemical energy compared with ideal structures having atomically abrupt interfaces. Therefore, multilayers fabricated with a large number of interfaces are comprised of a significant volume of premixed material and a measurable, reduced $|\Delta H_{rxn}|$. Of note, a reduced heat has been reported for several other multilayer systems when bilayer thickness is set to decananometer-scale dimensions [27–30].

The heats of reaction are plotted versus inverse bilayer thickness in order to establish the heat of formation (ΔH_o) for the Sc—Ag system. The data included in the inset plot of Fig. 5 are evaluated using the equation,

$$\Delta H_{rxn} = \Delta H_o - \Delta H_{premix}\left(\frac{2wV_{ScAg}}{t_B\, V_{premix}}\right), \quad (3)$$

which expresses ΔH_{rxn} in terms of the ΔH_o and the energy lost via preliminary reactions at interfaces. The terms in Eq. (3) include the enthalpy associated with formation of premixed amorphous volumes (ΔH_{premix}), the premixed thickness (w), the molar atomic volume of the product phase (V_{ScAg}), and the molar atomic volume of premixed regions (V_{premix}). The $|\Delta H_o|$ is the y-axis intercept of the inset plot. Extrapolating to this axis, one finds a value of $\Delta H_o = -24.3 \pm 1.2$ kJ/mol.at. that is similar to a previously-reported $\Delta H_o = -26.2$ kJ/mol.at [23].

3.3. Ignition temperatures

Each deposited multilayer was ignited via a hotplate. The T_{ig} varied from a low value of 260 °C for the 20.8 nm-bilayer multilayer to a value of 410 °C when t_B was set to 500 nm, as demonstrated in Fig. 6.

A logarithmic dependence on t_B, indicated with a fit line, is consistent with a recent model that was developed to explain thermal ignition of reactive nanolaminates and available experimental data [31]. Regarding the ignition model, Fritz and co-workers considered the power supplied by an external source, heat losses, and internal energy released during reaction to predict temperature evolution within a laminate [31]. Their approach led to an understanding that small period multilayers can be ignited at relatively lower temperature, because internal heat release is more efficient in materials having larger interface density and reduced effective diffusion lengths.

It is noted that the measured ignition temperatures of Sc/Ag multilayers are below the melting temperatures of elemental constituents (Ag, Sc), ScAg product, and other known Sc_xAg_y phases. This observation indicates that solid state mixing underlies initiation. In other words, liquid phase formation is not required to ignite Sc/Ag multilayers having nanometer-scale periodicity. This behavior is consistent with tests of other reactive, nanoscaled multilayers [29–33].

3.4. Three reaction modes observed in high-speed videography

3.4.1. Behavior of small bilayer thickness ($t_B < 100$ nm) Sc/Ag

Multilayer foils having a small period generally exhibited self-sustained, unstable reactions. Sc/Ag multilayers having a bilayer thickness of 20.8, 23.8, 27.8, 33.3, 41.7, 62.5, and 83.3 nm were tested in air and in vacuum, and all except one test resulted in a self-sustained, propagating reaction. Specifically, the thoroughly premixed 20.8 nm bilayer Sc/Ag did not react in vacuum.

Fig. 7(a) includes time-resolved images of a propagating reaction wave. This particular Sc/Ag multilayer, fabricated with a $t_B = 62.5$ nm, was tested in air. The multilayer is displayed in plan view which means that the individual reactant layers lie in the plane of the paper. Ignition has occurred outside the field of view, and the net reaction is moving left to right. The intermetallic wavefront is identified. Volumes to the right of the wavefront, which appear uniformly dark, are unreacted multilayer. Regions to the left of the intermetallic wavefront are reacting or have completed transformation. The mottled contrast in the reacting/reacted volumes is likely due to non-uniform heating. Additionally, buckling occurs in the product material soon after reaction and this leads to a non-uniform appearance as illuminating light moves out of a specular condition in local areas. Oxidation is not identified in the provided images although it is clearly evident as a bright wave in the full set of high-speed images. This second reaction occurs long after the passage of the intermetallic wave when reacted in air. In this particular test, the oxidation wave is positioned >1.5 mm behind the intermetallic wave.

The accompanying colored lines in Fig. 7(b) help identify the intermetallic wavefront position at the different times. Studying these boundaries shows that the wave does not advance uniformly in a stable mode. Instead, this example and the other specified multilayers undergo a spin instability. Reaction continues by the repeated passage of micro-scale bands along the boundary of previous reaction bands. The

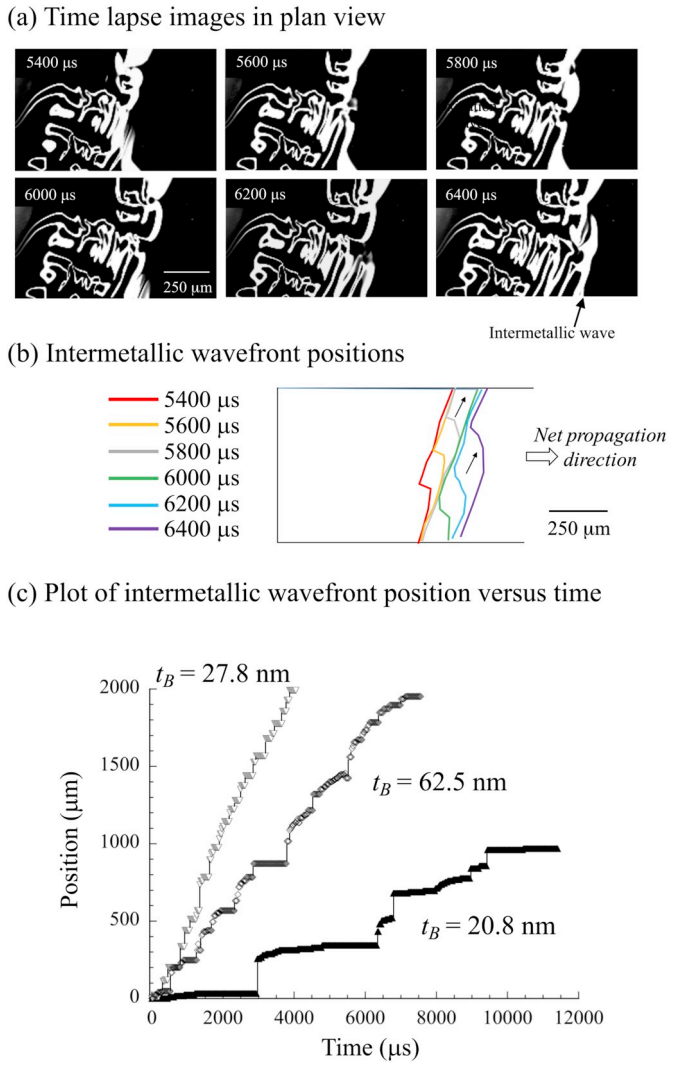


Fig. 7. (a) Image frames showing a propagating reaction in a Sc/Ag multilayer having a small t_B = 62.5 nm. The layers are positioned in plan view and net propagation direction is left-to-right. The trailing oxidation wave cannot be seen in this field. Corresponding wavefront maps in (b) were obtained from these same images. Plot of radial wavefront position versus time in (c) includes results for this and other small bilayer thickness Sc/Ag that exhibit unstable reactions when ignited in air.

bands travel adjacent to the previous reacted material in a direction that is roughly perpendicular to the net propagation direction. Arrows in Fig. 7(b) indicate the direction of two reaction bands that have widths of ~125 and 200 μm.

The plot of intermetallic wavefront positions in Fig. 7(c) further demonstrates this instability. In this figure, the radial position of three unstable waves is graphed versus time. A sudden increase in wavefront position, recognized as a step in Fig. 7(c), corresponds to the arrival of a new, microscopic spin band. After passing, the radial position of the reaction boundary is often unchanged until the arrival of another band. The wave has stalled in the net forward direction during this brief time.

The plot in Fig. 7(c) reveals a somewhat different behavior for the small bilayer thickness Sc/Ag multilayers. The instability appears minor in the 27.8 nm bilayer sample. Spin waves are evident in this specimen although the band widths are small. A detailed evaluation of high-speed videographs reveals a large spin band arrival rate for this sample. The spin instability is more pronounced in the 62.5 and 20.8 nm bilayer Sc/Ag multilayers; the arrival rate of spin bands is reduced and the times between band passage increased. The different unstable behaviors exhibited by these three multilayers are attributed to different internal heat release rates. Overall, one can interpret the average speeds of these different multilayers (considered the average slopes in position vs. time plots) as a measure of internal heat release rates. The Sc/Ag with t_B = 27.8 nm has a higher internal heat release rate than the multilayer with 62.5 nm bilayer. This difference is likely due to a reduced effective diffusion length associated with mass transport in the former. The more pronounced instability in the Sc/Ag with t_B = 20.8 nm is attributed to substantial energy loss via premixing. The overall heat release rate is reduced due to preliminary mixing/reaction of reactants along interfaces even though its multilayer period is the smallest of all tested samples. We note that similar behavior was found previously with Ni/Ti multilayers [18]. Multilayers exhibiting a maximum average propagating speed showed a less pronounced spin instability with reduced time between spin band passage compared with those having reduced internal heat release rate. Curiously, the Sc/Ag having t_B = 20.8 nm only propagated in air. We expect that this difference is also due to preliminary mixing of reactants and reduced heat of intermetallic reaction. Presumably, this single multilayer relies upon oxidation (specifically the energy boost provided by this secondary combustion reaction) to overcome the limited amount of stored chemical energy associated with the remaining metal reactant volumes. The overall trends of average speed in Sc/Ag multilayers are described later in this section.

Surrounding gaseous environment has little effect on these particular expanding intermetallic waves. Oxidation occurs long after the passage of the relatively-fast intermetallic wave in each of these multilayers when reacted in air. High-speed videography shows that the frequency of spin band passage is nominally the same for a given multilayer whether tested in air versus vacuum with the exception of the 20.8 nm-bilayer Sc/Ag which only propagates in air.

X-ray diffraction confirms that Sc_2O_3 is formed in samples that are reacted in air. X-ray diffractograms, such as the top one in Fig. 3, reveal a mixture of crystalline Sc_2O_3, $ScAg_2$, and Ag. The excess silver and lack of remaining Sc metal in air-reacted samples is attributed to the propensity of scandium to oxidize. Oxidation of Sc may further be enabled by the melt dissociation of Sc_xAg_y phases at high temperature. To be clear, although XRD demonstrates substantial oxidation when reaction is completed in air, high-speed videography clarifies that combustion occurs long after the passage of a self-sustained, intermetallic wave.

X-ray diffraction also shows that reactions in vacuum result in the formation of B2 ScAg product. There is no evidence of metal oxides or residual reactants after successful tests in vacuum. The middle diffractogram in Fig. 3 provides evidence for B2 ScAg along with trace $ScAg_2$ product.

3.4.2. *Behavior of intermediate bilayer thickness (100 < t_B < 200 nm) Sc/Ag*

Multilayer foils having intermediate bilayer thickness, with t_B between 100 and 200 nm, only reacted in air. No propagating reactions were observed when ignition was attempted in vacuum. Therefore, propagating reactions in these particular multilayers rely on the presence of air. Similar to the results in Fig. 3 (top diffractogram), XRD confirmed the formation of Sc_2O_3 in these particular multilayers. Thus, the reaction of oxygen and scandium is a key process that underlies these propagating reactions.

These particular reactions exhibit a complex oscillatory behavior comprised of both unstable and stable wave characteristics. A narrow reaction band passes along the boundary of previously-reacted material akin to the aforementioned 2-D spin instability. In Fig. 8(a) spin band passage is evident during the time between 7000 and 8000 μs. Soon after this time, the reaction wavefront presses forward in a uniform manner. The accompanying colored boundary lines in Fig. 8(b) show uniform advancement of the intermetallic front from 8500 to 9500 μs. Interestingly, high speed videography shows that oxidation is responsible for this advancing, stable mode. An oxidation reaction is

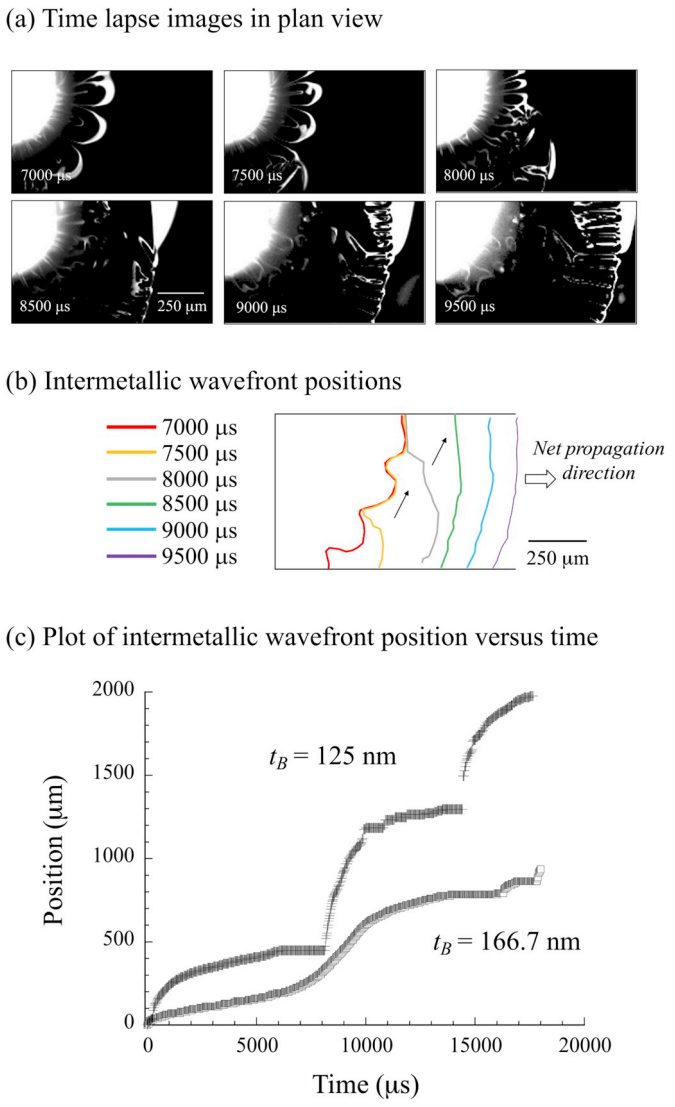


Fig. 8. (a) Image frames showing a propagating reaction in a Sc/Ag multilayer having an intermediate t_B = 125 nm. The layers are positioned in plan view and net propagation direction is left-to-right. The trailing oxidation wave is seen in this field. Corresponding wavefront maps in (b) were obtained from these same images. Plot of radial wavefront position versus time in (c) includes results for this and another intermediate bilayer thickness Sc/Ag that exhibits an alternating stable/unstable reaction wave when ignited in air.

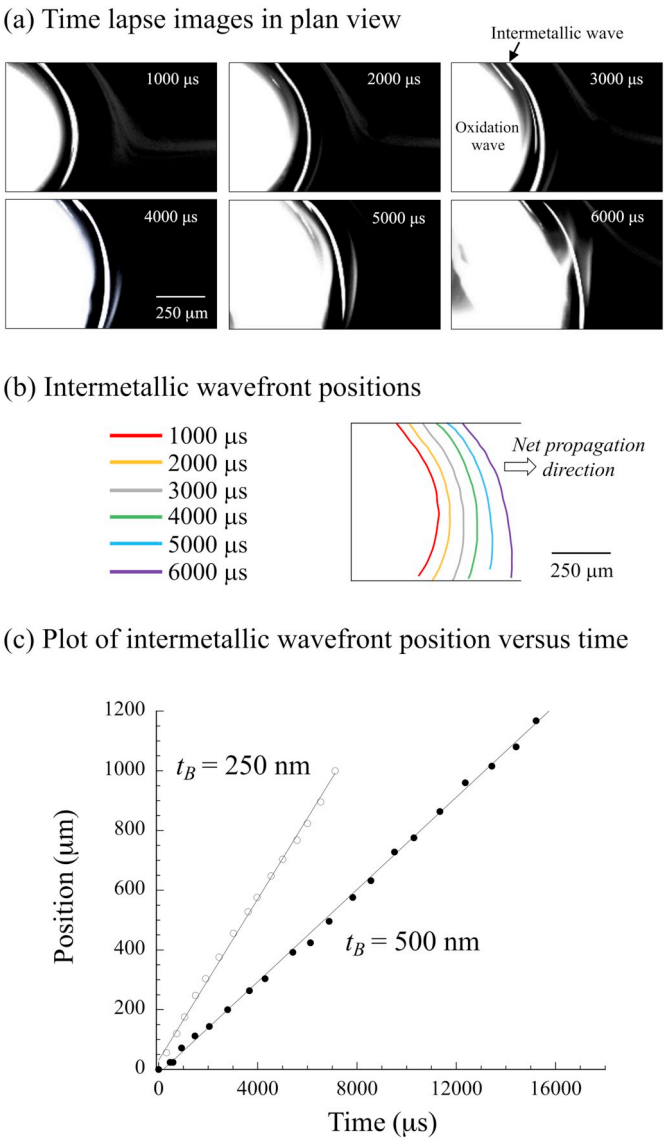


Fig. 9. (a) Image frames showing a propagating reaction in a Sc/Ag multilayer having a large t_B = 500 nm. The layers are positioned in plan view and net propagation direction is left-to-right. The trailing oxidation wave is seen in this field. Corresponding wavefront maps in (b) were obtained from these same images. Plot of radial wavefront position versus time in (c) includes results for two large bilayer thickness multilayers that exhibit stable propagation when reacted in air.

continually advancing behind the intermetallic front as evidenced by a relatively-bright wave in the high-speed images, and it ultimately moves close enough to impact the intermetallic reaction.

Oxidation is identified in Fig. 8(a) as a relatively bright feature that trails behind the intermetallic front. This second reaction first appears in the upper left hand corner of image 1 with the majority of the oxidizing volume appearing as a saturated feature in the image. The oxidation wavefront is not well defined. Instead, there is faint evidence of initial oxidation in front of the light-saturated (hottest) regions. Examination of this videograph shows that the oxidation reaction trails the intermetallic front by a distance that cycles between approximately 250 and 500 µm.

The position versus time plot in Fig. 8(c) further describes this complex series of events. A few rapid changes in position, assigned to the arrival of spin bands, are recognized. For example, the 125 nm-bilayer Sc/Ag exhibits a sudden increase in position at time ~8000 µs and again at 14000 µs. Different than the previously-described 2-D instabilities, the reaction wave continues to move forward between spin bands. Careful analysis of images shows a decreasing wavefront velocity during uniform advancement. The wave initially moves forward at a relatively high rate presumably due to the sudden influx of heat from prompt oxidation. However, after the intermetallic wave moves rapidly out ahead of the oxidation wave the former exhibits a decreased forward velocity. These unstable and stable characteristics alternate until the propagating wave reaches the far edge of the specimen.

3.4.3. Behavior of large bilayer thickness (t_B > 200 nm) Sc/Ag

Propagating reactions in large bilayer thickness Sc/Ag multilayers are also impacted by Sc oxidation. However, the reaction mode of the large bilayer thickness Sc/Ag is different than those having small or intermediate bilayer thicknesses. In all cases, the Sc/Ag with t_B > 200 nm exhibited stable propagating reactions with a smooth reaction wavefront. A stable wave is shown in Fig. 9(a, b). There is no evidence for spin bands in this particular multilayer or others fabricated with large t_B. Instead, the waves advance without interruption. A single

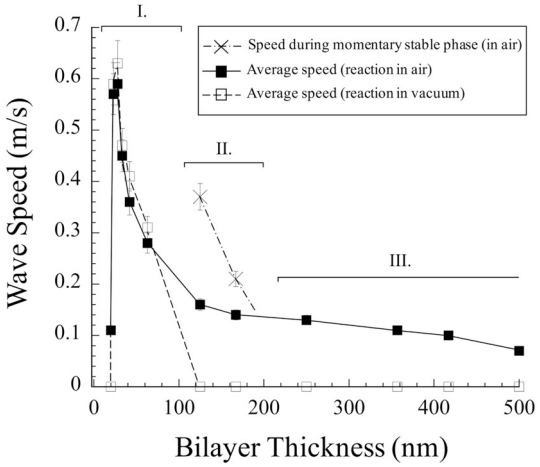


Fig. 10. Reaction wave speed of various Sc/Ag multilayers obtained from tests in vacuum (□) and in air (■). Additionally, the speed associated with waves temporarily stabilized by oxidation (×) are included. The three design regimes identified with roman numerals distinguish different reaction behaviors as follows. Zone I multilayers exhibit spin instabilities when tested in air or vacuum with no obvious interference from trailing oxidation waves (when reacted in air). Zone II multilayers undergo a complex oscillatory stable/unstable behavior when reacted in air; these same multilayers cannot be ignited in vacuum. Zone III multilayers only reacted in air and exhibited a stable reaction mode for the entire propagating event.

radial velocity characterizes each propagating wave as indicated by the linear slopes in Fig. 9(c). These multilayers do not react in vacuum.

The stability of propagating reaction waves is linked to prompt oxidation, confirming the original hypothesis. Oxidation occurs soon after the first reaction of Sc and Ag. In Fig. 9(a), oxidation is again recognized as a relatively bright feature originating on the left side of images. For this specimen, the oxidation reaction trails the intermetallic front by ~100 μm. Careful examination of captured videographs shows that the separation distance between intermetallic and oxidation fronts is reduced when t_B is increased from 250 to 500 nm. Although the oxidation wavefront once again appears broad, we find that this second reaction wave remains consistently closer to the intermetallic wave than for intermediate or small bilayer designs. Furthermore, its separation distance does not cycle or vary to the extent found in multilayers having intermediate t_B.

3.4.4. Wavefront speeds

The average wave speeds measured in the net forward direction are plotted in Fig. 10 for all three reaction modes (unstable, oscillatory, stable). The average reaction speed in air is represented with a filled symbol '■' whereas the average speed from testing in vacuum is represented with an unfilled '□'. Additionally, the wave speed has been measured during the temporarily-stabilized portion of reactions in intermediate designs. These particular speeds are represented with a '×'. The error bars represent a standard deviation with sources of error including frame and pixel resolution. Additionally, for the temporarily-stable portion of reactions, there is a range of instantaneous speeds which is captured in the error bars for these data. A zero speed indicates no sustained reaction.

These measurements show how intermetallic wave speed varies with gaseous environment and bilayer thickness. The effects of surrounding environment are most evident when evaluating multilayers having $t_B > 100$ nm. To reiterate, these particular multilayers only react when tested in air, whereas most Sc/Ag having bilayer thickness < 100 nm react in both air and vacuum. Looking closer at the results for small bilayer thickness Sc/Ag (zone I in Fig. 10), there is little difference between the average speeds when tested in vacuum versus air. It appears that the average wave speeds of the small bilayer thickness multilayers are slightly greater when tested in vacuum, yet experimental uncertainties make such a claim difficult. If real, this difference could be explained by the convective or conductive heat losses to surrounding gas compared with only radiation losses present in vacuum. As mentioned earlier, the 20.8 nm bilayer foil is an exception to this trend.

The change in average wave speeds with bilayer thickness are generally consistent with previous studies of reactive nanolaminates. Large bilayer thickness Sc/Ag multilayers are often characterized by low wave speeds. The speed generally increases as t_B is decreased due to an increased internal heat release rate. For Sc/Ag, this trend continues until a maximum velocity of 0.6 m/s is observed in multilayers having $t_B = 33$ nm. Multilayers having $t_B < 33$ nm propagate at lower speeds due to energy lost to premixing and decreased flame temperature (T_f).

4. Discussion

Insight into reaction mode and wave stability starts with a study of flame temperatures and examination of likely phase transformations. Propagating reactions fundamentally rely on the sudden, local release of energy and forward conduction of heat into unreacted volumes. Heat stimulates the mixing and reaction of internal species in neighboring volumes which advances a wave. The internal energy release solely gives rise to self-sustained, propagating reactions when material is successfully ignited in vacuum. Tests in air involve oxidation which can provide additional energy to the system. Specifically, a recent study shows that intermetallic compounds dissociate and metal oxides form to depths of 1–2 μm which provides substantial extra energy beyond that associated with intermetallic formation [34].

The high temperatures attained during a propagating reaction are derived from the enthalpy difference between reactants and products. An enthalpy-temperature diagram is therefore beneficial for visualizing the thermodynamics underlying a reaction and the transformations that may occur [35,36]. The diagram presented in Fig. 11 includes two curves that describe ScAg formation. The upper (red) curve represents the enthalpy of reactants, whereas the bottom (blue) one denotes the enthalpy of ScAg product. A difference at a particular temperature represents the enthalpy change associated with the formation of ScAg. The plot is generated from a combination of measured and archived information listed in Table 2. For example, the enthalpy difference at 22 °C is set to the ΔH_o determined in this study to be −24.3 kJ/mol.at. (−317 J/g). Except at phase transformations, the slopes are represented by the specific heat capacity (c_p) of the various materials [37]. The mass-weighted c_p of the two reactants is set to 0.335 J/g °C, and a value for $c_p = 0.421$ J/g °C [38] is used for the product curve. Phase transformations, including melting, vaporization and a solid transformation of Sc, are recognized by sudden changes in enthalpy at specific temperatures [37,39,40,41]. The product phase ScAg melts at 1230 °C [40] and the enthalpy change (636.6 J/g) [38] of the product at this temperature corresponds to its latent heat of melting, ΔH_{fus}.

A few other relevant temperatures are identified in the enthalpy-temperature diagram. The adiabatic value (T_a) is estimated by assuming all heat of formation is transferred to product. This temperature is determined by drawing a horizontal tie line from the ambient temperature (T_o) value on the reactant enthalpy curve to a point of intersection on the product curve as shown. Reactions are certainly affected by energy losses. This can manifest in the form of chemical potential energy lost due to premixing as well as energy lost dynamically by conduction, radiation and/or convection. As a result, the flame will attain a lower T_f.

Flame temperatures are first estimated for formation reactions by applying the measured, multilayer-specific ΔH_{rxn} that, in effect, accounts for energy lost to premixing. The first example shown in Fig. 11 with dashed lines describes a 125 nm-bilayer Sc/Ag multilayer. For this case, the flame temperature is estimated to be below the melting temperatures of ScAg product, Sc (1541 °C), and Ag (962 °C). The flame

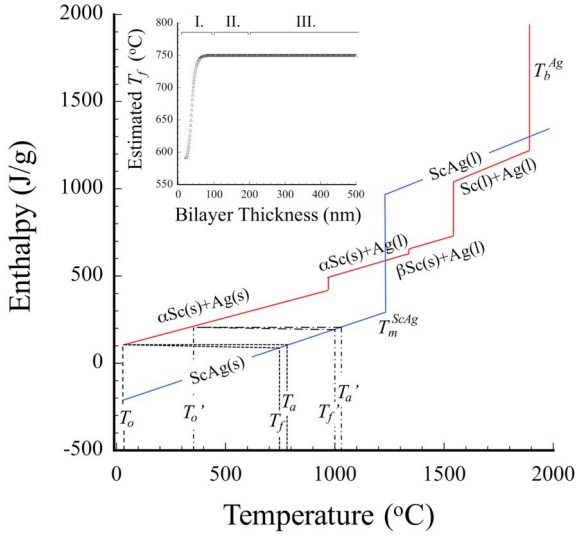


Fig. 11. Enthalpy-temperature diagram for Sc + Ag - > ScAg. Red curve represents enthalpy of reactants and blue curve displays the enthalpy of product. Example reactions in the 125 nm-bilayer Sc/Ag are described with dashed and dotted lines. The first set of lines represent a multilayer that is maintained at ambient value (T_o) prior to reaction. The sample reacts to a flame temperature (T_f) that is less than the adiabatic value (T_a). With a second set of lines, one visualizes the effects of preheating to a different initial temperature (T_o') > T_o. The shown example sets T_o' = 350 °C and this leads to a higher T_f' and adiabatic value, T_a'. The notations (s) and (l) refer to solid and liquid phases, respectively. The T_f s included in the inset plot are estimated from the enthalpy-temperature diagram when applying the ΔH_{rxn} at T_o. The zone numbers listed at the top of this inset plot identify the mode described earlier with Fig. 10. (For interpretation of the references to colour in this figure legend, the reader is referred to the web version of this article.)

Table 2
Material properties used in the construction of the ScAg enthalpy-temperature diagram included in Fig. 11. Values for c_p are specified at 25 °C and 100 kPa. T_b = boiling temperature. ΔH_{vap} = heat of vaporization. n/k = not known or identified.

	Sc	Ag	ScAg	References
ΔH_o (J/g)	–	–	−317	this study
c_p (J/g °C)	0.568	0.235	0.421	37, 38
T_m (°C)	1541	961.78	1230	37, 39, 40
ΔH_{fus} (J/g)	313	104	636.6	37, 38
T_b (°C)	2836	2162	n/k	37
ΔH_{vap} (J/g)	8390 kJ/mol	2360	n/k	37, 41

temperatures of the various Sc/Ag multilayers estimated using this approach are included with an inset plot in Fig. 11. This additional plot shows that all T_fs lie well below the melting points of product, reactants, and various known intermetallics.

It is interesting that propagating reactions occur in a few of the smallest t_B multilayers even though flame temperatures are calculated to be less than the melting temperatures of reactants, product, etc. Propagating reactions that occur in vacuum are self-sustained (i.e., these occur without a boost from Sc oxidation). This implies that either a solid flame occurs in the Sc/Ag system, or there is an alternate path to propagating, formation reactions.

It is intriguing to consider whether the unstable behavior observed in fine bilayer Sc/Ag somehow overcomes the low enthalpy difference. One speculates whether the heat pushed forward from a stalled front could contribute to the passage of a spin band by locally raising the temperature ahead of its arrival. If heating occurs ahead of a spin band, the local flame temperature of the spin band could be higher than the previous estimate. Evidence for preheating ahead of a stalled front has been reported for the unstable Co/Al multilayer system [11]. Thus, such an effect seems feasible and its ramifications deserve study.

Questions then arise as to whether preheating could help elevate the local flame temperature of a passing spin band to the melting temperature (T_m) of Ag - the reactant with lowest T_m. The formation of a liquid reactant or liquid product phase is generally expected to increase diffusivity in reactive materials. Previous studies of other multilayer systems demonstrate markedly increased mixing kinetics in reactive nanolaminates when at least one reactant melts [33,42,45]. If correct, the continued passage of reaction bands in Sc/Ag multilayers could be tied to the melting of Ag achieved by the combined effects of preheating and propagating reactions. The T_f shown in Fig. 11 is estimated using no additional preheating above room temperature, and, yet, this value lies only ~200 to 300 °C below the T_m of Ag. Therefore, modest preheating could potentially lead to a different phase pathway.

With an interest in whether the heat pushed forward ahead of a stalled front contributes to the continued propagation of reaction bands, we have measured the spin band widths and compared these to the thermal lengths ahead of a stalled wave estimated by a heat conduction model. Specifically, our thermal model uses the time-dependent heat equation,

$$\frac{d^2T}{dr^2} = \frac{1}{a}\left(\frac{dT}{dt}\right), \tag{4}$$

to examine the heat flow from a stationary hot wall (set at silver melt) in to neighboring unreacted volumes. The notion of maintaining a hot wall at a fixed temperature seems reasonable based on past high speed thermal imaging that showed reacted material near a stalled front remaining at a substantial, elevated value for a time that was long compared with the observed duration between band passage [11]. The time (t) evolution of temperature (T) is estimated for different distances (r) in the radial direction. In this equation, a is the in-plane thermal diffusivity of layered reactants set equal to 64 W/m °C [43]. The generated thermal profiles are then used to calculate modified, local flame temperatures (T_f') for a passing spin band as a function of distance from the stalled boundary. The calculated lengths, referred to as 'Ag melt position' in Fig. 12, are the radial distances over which Ag is expected to melt as a result of the combined effects. These distances are calculated for different times referenced to the arrival of the previous spin band (i.e., hot wall). One can understand the path to localized silver melting by returning to the ScAg enthalpy-temperature diagram in Fig. 11. Heat flow calculations reveal local temperatures (T_o') ahead of a stalled front that can exceed the ambient T_o. The second example shown in Fig. 11

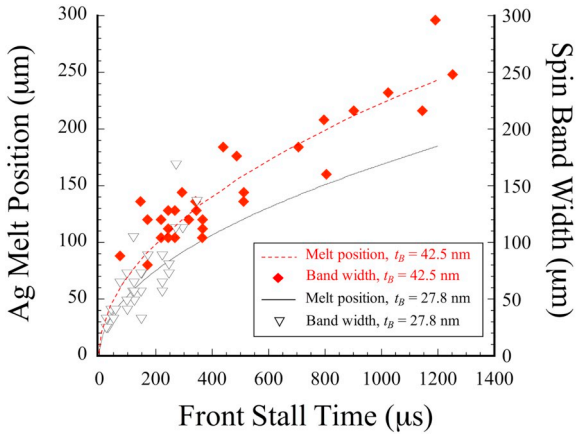


Fig. 12. Scatter plot of measured spin band width for two fine bilayer Sc/Ag multilayers and corresponding times-since-band-passage (referred to as 'Front stall time'). The lines show predicted distances of molten Ag in front of stalled waves. These distances are calculated from the enthalpy change for Sc + Ag - > ScAg for spin bands propagating into volumes preheated for different times.

with dashed-dotted lines starts with a T_o' = 350 °C to reflect the larger values obtained from model calculations. Applying the measured ΔH_{rxn} to the enthalpy diagram at this revised temperature leads to a higher flame temperature, T_f', = 1000 °C. Of note, this is slightly greater than the Ag melt point (identified on the red reactant curve).

Overall, the measured spin band widths obtained from high-speed videography correlate reasonably well to the predicted positions of Ag melt for small t_B multilayers. Fig. 12 includes a scatter plot of the measured spin band widths for two multilayers (with t_B = 27.8, 42.5 nm) and the corresponding times-since-band-passage (referred to as 'Front stall time'). The experimental measurements show considerable variation in band width and stall time, yet trends emerge for both multilayers that are consistent with model calculations of melt position. The spin band width generally increases with stall time. This can be explained by additional heat spreading with time and attainment of higher local temperatures.

Correlation of these two dimensions is considered evidence for preheating effects on propagating spin waves. The calculations show that preheating can elevate local temperatures in unreacted volumes such that the passing spin band flame temperature can reach the T_m of one reactant (Ag). Knowing that reactant melting can enable rapid mass transport in formation reactions [44], we surmise that preheating could be a key ingredient to the continued, unstable propagation for these particular Sc/Ag multilayers.

If correct, a question remains about the lack of self-propagating reactions in large-bilayer thickness multilayers associated with zones II and III. Initial estimates of their flame temperatures are also below the T_m of silver. A mechanism for quenching a stable front is understood to involve a heat sink, such as a substrate [45], that can remove enough heat from the reaction zone to inhibit mass transport. For a freestanding foil, the heat is lost into the reactants. This condition is most likely to occur in a multilayer system when bilayer thickness is at its largest due to both the longer transverse diffusion distances necessary for reaction and higher longitudinal thermal conductivity predicted by thermal circuit models. Consequently, spin mode propagation in vacuum appears to require both preheating from forward heat transfer and sufficiently small diffusion lengths to propagate given the diffusivity of liquid Ag.

Finally, a switch from an unstable wave to a stable reaction front in large bilayer Sc/Ag is indicative of changing from a time-dependent flame temperature to a time-independent one [2,13]. Additionally, this mode is consistent with the functional form and wave speed dependence put forth in a model by Mann et al. that describes propagating reactions in energetic nanolaminates [46]. Heat flux, dQ/dt, provided to an intermetallic front by the oxidation of Sc is a function of separation distance and time. Considering the oxidation front as an inertial reference frame, the same functional form of heat diffusion into a semi-infinite body used to describe flux from a stalled band into neighboring reactants (to help define the subsequent band) can be applied to evaluate heat flow from the oxidation reaction into ScAg product.

Given that the stable front velocities for the 125, 250, 317, and 457 nm bilayer Sc/Ag are faster than the oxidation front velocity (0.07 m/s), one expects a stable regime that maintains a constant T_f at the intermetallic front over a range of heat fluxes. Such a condition is met at the melt isotherm of the ScAg product phase.

To test this hypothesis, a contrived case in which the oxidation-assisted reaction kinetics at the intermetallic front produce the same velocity as the oxidation wave was considered. This occurs experimentally for the 500 nm-thick bilayer Sc/Ag giving an opportunity to compare. From the reference frame of the oxidation wavefront, this case can be treated as a steady state heat diffusion channel of length, L, with a hot wall at the oxidation front temperature (T_{ox}) and cold wall at the intermetallic flame temperature (T_f) described by the equation,

$$\frac{dQ}{dt} = \frac{-\kappa_{ScAg}(T_f - T_{ox})}{L}, \quad (5)$$

wherein the thermal conductivity of the product phase (κ_{ScAg}) is estimated from the literature to be 50 W/m °C [47,48]. The T_{ox} is estimated by considering the energy added to the system by this reaction. Cross-section EDS of samples reacted in air show scandium oxide forming to a depth of ~1 μm on both sides of a reactive Sc/Ag foil once reaction is complete. Considering the substantial heat of formation for $4Sc + 3O_2 -> 2Sc_2O_3$ (−20.9 kJ/g) [49] applied to these limited volumes of material, a material-specific, enthalpy-temperature diagram is used to predict an T_{ox} that reaches the T_b of Ag (2162 °C) [50–53]. The T_f of the intermetallic front is then determined by solving for a heat flux at which the Sc/Ag enthalpy-temperature diagram produces a reaction front temperature equal to the cold wall temperature. This solution occurs at the melt temperature of ScAg.

5. Conclusions

Rare-earth/transition metal multilayers undergo propagating, high-temperature formation reactions. Small period Sc/Ag multilayers having a bilayer thickness < 100 nm exhibit relatively fast, self-sustained reactions that are largely unaffected by gaseous environment. Sc/Ag multilayers having a bilayer thickness > 100 nm rely on secondary reactions of Sc and O to continue propagating reactions; these particular materials do not react in vacuum. Whereas the small period Sc/Ag multilayers undergo unstable propagating reactions, two unique modes are identified for large period Sc/Ag multilayers. Those having a bilayer thickness in the range of approximately 100 to 200 nm exhibit characteristics of both stable and unstable reaction waves. This newly-discovered oscillatory behavior involves the passage of narrow, unstable reaction bands followed by the uniform advancement of a reaction wave driven, in large part, by the heat of scandium oxidation. This series of events repeats giving rise to an alternating unstable/stable mode. Sc/Ag multilayers having large bilayer thickness, in excess of ~200 nm, develop uniform propagating waves. These particular reactions are stabilized by prompt oxidation of scandium and the influx of added energy associated with this secondary reaction. In this case, the stable forward reaction wave is characterized by a smooth wavefront morphology and constant speed along a radial direction.

Wavefront temperatures have been estimated using archived properties and measured heats of reaction. These calculations indicate that the maximum flame temperature of unassisted intermetallic reactions (meaning no oxidation and no preheating above room temperature) is below the melt temperatures of Ag, Sc and various Sc_xAg_y phases. A thermal spreading model shows that significant preheating can occur slightly ahead of a stalled wave and potentially raises the local spin band flame temperature to the melt point of Ag in some designs. Good correlation of predicted silver melt distances and measured spin band widths leads to a proposed explanation for 2-D instabilities occurring in small bilayer thickness designs. Namely, the extra energy provided by conduction ahead of a stalled wavefront preheats volumes into which reaction bands propagate. The local flame temperature is elevated to the melt point of silver, therein providing a favorable kinetic pathway for self-sustained (albeit unstable) propagating reactions. Reactions in large bilayer thickness multilayers are unable to maintain a propagating (stable or unstable) reaction without assistance from oxidation. These propagating reactions rely on heat pushed forward by a neighboring, prompt oxidation reaction. Thermodynamic considerations point to an intermetallic wave temperature equal to the melt point of ScAg product for these particular reactions.

In summary, our study demonstrates many complexities that arise from competing chemical reactions (intermetallic versus secondary oxidation) in reactive multilayers. The different reactions occur at various rates which are linked to elements of material design. These findings should assist those developing applications that require detailed knowledge of energy output, for secondary oxidation reactions can provide a substantial exothermic boost to certain reactive metal systems. Furthermore, prompt oxidation provides an alternate approach

for examining wave stability criteria in these emerging reactive materials.

Acknowledgements

The authors would like to thank D.L. Perry, P. Kotula, J.P. McDonald, R.V. Reeves, C. Saltonstall, and T. Beechem for technical support and discussions. Supported by the Laboratory Directed Research and Development program at Sandia National Laboratories, a multimission laboratory managed and operated by National Technology and Engineering Solutions of Sandia, LLC., a wholly owned subsidiary of Honeywell International, Inc., for the U.S. Department of Energy's National Nuclear Security Administration under contract DE-NA-0003525. This paper describes objective technical results and analysis. Any subjective views or opinions that might be expressed in the paper do not necessarily represent the views of the U.S. Department of Energy or the United States Government.

References

[1] A.S. Rogachev, J.-C. Gachon, H.E. Grigoryan, A.N. Nosyrev, P.A. Tsygankov, J.C. Schuster, D. Vrel, Phase evolution during gasless combustion of the micro-and nano-heterogeneous systems: time resolved study by synchrotron radiation diffraction analysis, Nucl. Instr. Meth. Phys. Res. A 543 (2005) 175–179.
[2] C.E. Wickersham, G. Bajor, J.E. Greene, Impulse stimulated “explosive” crystallization of sputter deposited (In,Ga)Sb films, Solid State Comm. 27 (1978) 17–20.
[3] S.V. Krishnaswamy, R. Messier, P. Swab, L.L. Tongson, Explosive crystallization of rf-sputtered amorphous CdTe films, J. Elect. Mat. 10 (1981) 433–443.
[4] H.J. Leamy, W.L. Brown, G.K. Celler, G. Foti, G.H. Gilmer, J.C.C. Fan, Explosive crystallization of amorphous germanium, Appl. Phys. Lett. 38 (1998) 137.
[5] J.A. Floro, Propagation of explosive crystallization in thin Rh-Si multilayer films, J. Vac. Sci. Technol. A 4 (1986) 631–638.
[6] E. Ma, C.V. Thompson, L.A. Clevenger, K.N. Tu, Self-propagating explosive reactions in Al/Ni multilayer thin films, Appl. Phys. Lett. 57 (1990) 1262–1264.
[7] J.C. Trenkle, L.J. Koerner, M.W. Tate, N. Walker, S.M. Gruner, T.P. Weihs, T.C. Hufnagel, Time-resolved X-ray microdiffraction studies of phase transformations during rapidly propagating reactions in Al/Ni and Zr/Ni multilayer foils, J. Appl. Phys. 107 (2010) 113511.
[8] J.C. Trenkle, J. Wang, T.P. Weihs, T.C. Hufnagel, Microstructural study of an oscillatory formation reaction in nanostructured reactive multilayer foils, Appl. Phys. Lett. 87 (2005) 153108.
[9] J.P. McDonald, V.C. Hodges, E.D. Jones Jr., D.P. Adams, Direct observation of spinlike reaction fronts in planar energetic multilayer foils, Appl. Phys. Lett. 94 (2009) 034102.
[10] S.C. Barron, S.T. Kelly, J. Kirchhoff, R. Knepper, K. Fisher, K.J.T. Livi, E.M. Dufresne, K. Fezzaa, T.W. Barbee, T.C. Hufnagel, T.P. Weihs, Self-propagating reactions in Al/Zr multilayers: anomalous dependence of reaction velocity on bilayer thickness, J. Appl. Phys. 114 (2013) 223517.
[11] R.V. Reeves, D.P. Adams, Reaction instabilities in Co/Al nanolaminates due to chemical kinetics varying over micron-scales, J. Appl. Phys. 115 (2014) 044911.
[12] G.C. Egan, T.T. Li, J.D. Roehling, J.T. McKeown, G.H. Campbell, In-situ dynamic TEM characterization of unsteady crystallization during laser processing of amorphous germanium, Acta Mater. 143 (2017) 093512.
[13] W. Van Saarloos, J.D. Weeks, Surface undulations in explosive crystallization: a thermal instability, Phys. Rev. Lett. 51 (1983) 1046–1049.
[14] D.A. Kurtze, W. Van Saarloos, J.D. Weeks, Front propagation in self-sustained and laser-driven crystal growth: stability analysis and morphological aspects, Phys. Rev. B 30 (1984) 1398–1415.
[15] S. Jayaraman, O.M. Knio, A.B. Mann, T.P. Weihs, Numerical predictions of oscillatory combustion in reactive multilayers, J. Appl. Phys. 86 (1999) 800–809.
[16] L. Alawieh, O.M. Knio, T.P. Weihs, Effect of thermal properties on self-propagating fronts in reactive nanolaminates, J. Appl. Phys. 110 (2011) 013409.
[17] C.E. Wickersham, G. Bajor, J.E. Greene, Temperature dependent formation of surface undulations in explosively crystallized films, J. Vac. Sci. Technol. A 3 (1985) 336–338.
[18] J.P. McDonald, R.V. Reeves, E.D. Jones Jr., K.A. Chinn, D.P. Adams, Effects of oxidation on reaction front instabilities and average propagation speed in Ni/Ti multilayer foils, J. Appl. Phys. 113 (2013) 103505.
[19] R.V. Reeves, M.A. Rodriguez, E.D. Jones Jr., D.P. Adams, Condensed-phase and oxidation reaction behavior of Ti/2B foils in varied gaseous environments, J. Phys. Chem. C 116 (2012) 17904–17912.
[20] H. Joress, S.C. Barron, K.J.T. Livi, N. Aronhime, T.P. Weihs, Self-sustaining oxidation initiated by rapid formation reactions in multilayer foils, Appl. Phys. Lett. 101 (2012) 111908.
[21] J.P. McDonald, M.A. Rodriguez, E.D. Jones Jr., D.P. Adams, Rare-earth transition-metal intermetallic compounds produced via self-propagating, high-temperature synthesis, J. Mater. Res. 25 (2010) 718–727.
[22] E.J. Huber Jr., C.E. Holley, The heat of formation of scandium oxide, J. Phys. Chem. 67 (1963) 1731.
[23] K. Fitzner, W.-G. Jung, O.J. Kleppa, Thermochemistry of binary alloys of transition metals: the Me-Sc, Me-Y, and Me-La (Me = Ag, Au) systems, Metall. Trans. A. 22A (1991) 1103–1111.
[24] C. Colinet, The thermodynamic properties of rare earth metallic systems, J. Alloys Compd. 225 (1995) 409–422.
[25] H.E. Kissinger, Variation of peak temperature with heating rate in differential thermal analysis, J. Res. Natl. Bur. Stand. 57 (1956) 217–221.
[26] C. Michaelsen, K. Barmak, T.P. Weihs, (Review article) investigating the thermodynamics and kinetics of thin film reactions by differential scanning calorimetry, J. Phys. D. Appl. Phys. 30 (1997) 3167–3186.
[27] D.P. Adams, Reactive multilayers fabricated by vapor deposition: a critical review, Thin Solid Films 576 (2015) 98–128.
[28] A.J. Gavens, D. Van Heerden, A.B. Mann, M.E. Reiss, T.P. Weihs, Effect of intermixing on self-propagating exothermic reactions in Al/Ni nanolaminate foils, J. Appl. Phys. 87 (2000) 1255–1263.
[29] D.P. Adams, M.A. Rodriguez, J.P. McDonald, M.M. Bai, E. Jones Jr., L. Brewer, J.J. Moore, Reactive Ni/Ti nanolaminates, J. Appl. Phys. 106 (2009) 093505.
[30] D.P. Adams, V.C. Hodges, M.M. Bai, E. Jones Jr., M.A. Rodriguez, T. Buchheit, J.J. Moore, Exothermic reactions in Co/Al nanolaminates, J. Appl. Phys. 104 (2008) 043502.
[31] G.M. Fritz, S.J. Spey Jr., M.D. Grapes, T.P. Weihs, Thresholds for igniting exothermic reactions in Al/Ni multilayers using pulses of electrical, mechanical, and thermal energy, J. Appl. Phys. 113 (2013) 014901.
[32] K.V. Manukyan, B.A. Mason, L.J. Groven, Y.-C. Lin, M. Cherukara, S.F. Son, A. Strachan, A.S. Mukasyan, Tailored reactivity of Ni + Al nanocomposites: microstructural correlations, J. Phys. Chem. C 116 (2012) 21027–21038.
[33] D.P. Adams, R.V. Reeves, M.J. Abere, C. Sobczak, C.D. Yarrington, M.A. Rodriguez, P.G. Kotula, Ignition and self-propagating reactions in Al/Pt multilayers of varied design, J. Appl. Phys. 124 (2018) 095105.
[34] S. Sen, M. Lake, P. Schaaf, Experimental investigation of high temperature oxidation during self-propagating reaction in Zr/Al reactive multilayer films, Surf. Coat. Tech. 340 (2018) 66–73.
[35] J.J. Moore, H.J. Feng, Combustion synthesis of advanced materials: part I. reaction parameters, Prog. Mater. Sci. 39 (1995) 243–273.
[36] J.J. Moore, H.J. Feng, Combustion synthesis of advanced materials: part II. Classification, applications, and modeling, Prog. Mater. Sci. 39 (1995) 275–316.
[37] W.M. Haynes, CRC Handbook of Chemistry and Physics, 96th ed. CRC Press, Boca Raton, 2015.
[38] J.O. Andersson, T. Helander, L. Hoglund, P.F. Shi, B. Sundman, Thermo-Calc and DICTRA, computational tools for materials science, Calphad 26 (2002) 273–312.
[39] K.A. Gschneidner Jr., A.O. Tsokol, V.K. Pecharsky, A.M. Russell, Intermetallic Articles of Manufacture Having High Room Temperature Ductility, United States Patent Application US 2005/0274439, Dec, vol. 15, (2005).
[40] I. Stapf, G. Kiessler, E. Gebhardt, Das system silber-scandium, J. Less-Common Metals 39 (1975) 219–225.
[41] H.M. Schadel Jr., C.E. Birchenall, The vapor pressure of silver, JOM 2 (1950) 1134–1138.
[42] M.J. Abere, C.D. Yarrington, D.P. Adams, Heating rate dependent ignition of Al/Pt nanolaminates through pulsed laser irradiation, J. Appl. Phys. 123 (2018) 235304.
[43] The Value for α Is Calculated from Thermal Conductivity (κ) Measured by Frequency Domain Thermoreflectance (FDTR), the Average Heat Capacity (c_p) of the Reactants, (and Average density (ρ) According to the Relationship: $\alpha = \kappa/(\rho c_p)$).
[44] A.S. Rogachev, A.S. Mukasyan, Combustion of heterogeneous nanostructural systems (review), Combust. Explosion Shock Waves 46 (2010) 243–266.
[45] D.E. Kittell, C.D. Yarrington, M.L. Hobbs, M.J. Abere, D.P. Adams, A diffusion-limited reaction model for self-propagating Al/Pt multilayers with quench limits, J. Appl. Phys. 123 (2018) 145302.
[46] A.B. Mann, A.J. Gavens, M.E. Reiss, D. Van Heerden, G. Bao, T.P. Weihs, Modeling and characterizing the propagation velocity of exothermic reactions in multilayer foils, J. Appl. Phys. 82 (1997) 1178–1188.
[47] E. Bauer, E. Gratz, H. Nowotny, Transport properties and electronic structure of nonmagnetic REAg compounds, Z. Phys. B Condens. Matter 64 (1986) 151–158.
[48] S. Rameshkumar, V. Jayalakshmi, G. Jaiganesh, An ab-initio study of electronic and thermodynamic properties of Ag-Sc intermetallics, High Temperautres – High Pressures, vol. 47, 2018, pp. 165–177.
[49] J.E. Huber Jr., G.C. Fitzgibbon, E.L. Head, C.E. Holley Jr., The heat of formation of scandium oxide, J. Phys. Chem. 67 (1963) 1731–1733.
[50] Y. Zhang, Thermodynamic Properties of Rare Earth Sesquioxides, PhD Dissertation McGill University, 2016.
[51] K.A. Gschneidner Jr., F.W. Calderwood, The Ag-Sc (silver-scandium) system, Bull. Alloy Phase Diagr. 4 (1983) 375–377.
[52] E.E. Shpil'rain, D.N. Kagan, L.S. Barkhatow, V.V. Koroleva, J.P. Coutures, M. Foex, Investigation of fusion and phase transition enthalpies of Y_2O_3 and Sc_2O_3, Rev. Int. Hautes Temp. Refract. 15 (1978) 249–252.
[53] E.E. Shpil'rain, D.N. Kagan, L.S. Barkhatov, L.I. Zhmakin, V.V. Koroleva, Combined study of the thermophysical and electrophysical properties of rare-earth sesquioxides in solid and liquid phases, High Temperatures-High Pressures 11 (1979) 539–542.